

RESEARCH

Open Access



APOL6 predicts immunotherapy efficacy of bladder cancer by ferroptosis

Zhiwei Fan^{1,2,3†}, Yiting Liu^{1,2,4†}, Xuehai Wang^{2†}, Yuting Xu¹, Ruiyao Huang², Weijian Shi², Yi Qu², Jialing Ruan², Chu Zhou², Xinyuan Zhao^{2*} and Lei Liu^{1*}

Abstract

Background Immune checkpoint inhibitors (ICIs) are rapidly evolving in the management of bladder cancer (BLCA). Nevertheless, effective biomarkers for predicting immunotherapeutic outcomes in BLCA are still insufficient. Ferroptosis, a form of immunogenic cell death, has been found to enhance patient sensitivity to ICIs. However, the underlying mechanisms of ferroptosis in promoting immunotherapy efficacy in BLCA remain obscure.

Methods Our analysis of The Cancer Genome Atlas (TCGA) mRNA data using single sample Gene Set Enrichment Analysis (ssGSEA) revealed two immunologically distinct subtypes. Based on these subtypes and various other public cohorts, we identified Apolipoprotein L6 (APOL6) as a biomarker predicting the efficacy of ICIs and explored its immunological correlation and predictive value for treatment. Furthermore, the role of APOL6 in promoting ferroptosis and its mechanism in regulating this process were experimentally validated.

Results The results indicate that APOL6 has significant immunological relevance and is indicative of immunologically hot tumors in BLCA and many other cancers. APOL6, interacting with acyl-coenzyme A synthetase long-chain family member 4 (ACSL4), mediates immunotherapy efficacy by ferroptosis. Additionally, APOL6 is regulated by signal transducer and activator of transcription 1 (STAT1).

Conclusions To conclude, our findings indicate APOL6 has potential as a predictive biomarker for immunotherapy treatment success estimation and reveal the STAT1/APOL6/GPX4 axis as a critical regulatory mechanism in BLCA.

Keywords APOL6, Bladder cancer (BLCA), Immunotherapy, Ferroptosis

[†]Zhiwei Fan, Yiting Liu and Xuehai Wang contributed equally to this work.

*Correspondence:

Xinyuan Zhao
zhaoxinyuan@ntu.edu.cn

Lei Liu
liulei19920123@163.com

¹ Department of Pathology, Affiliated Hospital of Nantong University, Medical School of Nantong University, Nantong 226006, China

² Department of Occupational Medicine and Environmental Toxicology, Nantong Key Laboratory of Environmental Toxicology, School of Public Health, Nantong University, Nantong 226019, China

³ Department of Urology and Andrology, Sir Run Run Shaw Hospital, Zhejiang University School of Medicine, Hangzhou 310016, China

⁴ Department of Interventional Radiology, Ruijin Hospital, Shanghai Jiao Tong University School of Medicine, Shanghai 200025, China

Introduction

Bladder cancer (BLCA) is a significant global health concern, ranking as the tenth most common diagnosed cancer, with approximately 83,190 incident cases and 16,840 deaths reported occurring worldwide each year [1]. The standard first-line treatment for BLCAs involves platinum-based chemotherapy, specifically cisplatin or carboplatin. However, only a minority of patients experience long-term benefits from this treatment [2, 3].

In contrast to traditional chemotherapy and radiation therapy, cancer immunotherapy has made significant strides in research and offers a novel approach to treating malignant tumors [4]. This therapy enhances the patient's immune response to attack cancer cells, primarily through targeting tumor cell immune evasion



mechanisms [5]. The most promising avenue in immunotherapy involves blocking immune checkpoints on both tumor and anti-tumor immune cells by employing immune checkpoint inhibitors (ICIs) [6]. The interplay of programmed cell death ligand 1 (PD-L1) on tumor cells and programmed cell death 1 (PD1) on immune cells combating cancer plays a key role in tumor immune evasion [7]. Inhibiting this interaction with ICIs presents a promising strategy for targeted tumor immunotherapy [8]. BLCA, characterized by a high mutational burden, is particularly amenable to immunotherapy, especially with checkpoint inhibitors targeting PD-1 and its ligand, PD-L1 [9]. The US Food and Drug Administration (FDA) and the European Medicines Agency (EMA) have approved Atezolizumab and Pembrolizumab, two PD-1 or PD-L1 inhibitors, as first-line treatments for cisplatin-ineligible patients with positive PD-L1 status [2, 10]. Although PD-L1 positivity suggests a clinical benefit [11], numerous patients exhibiting negative PD-L1 expression have also shown responses to immunotherapy [12]. Thus, the sole reliance on PD-L1 detection is inadequate for selecting patients for immunotherapy, highlighting the urgent need for alternative biomarkers in clinical practice to predict responses to immunotherapy.

The tumor immune microenvironment (TME) represents a multifaceted and diverse cellular landscape that significantly influences tumor growth [13, 14]. This environment is characterized by a dynamic extracellular matrix (ECM) and a diverse range of secreted factors, including cytokines, growth factors, and chemokines. Tumors are informally categorized based on the TME as either immune “cold,” characterized by an immunosuppressive milieu, or immune “hot,” distinguished by the presence of tumor-infiltrating lymphocytes (TILs), elevated PD-L1 expression on tumor-associated immune cells, potential genomic instability, and existing anti-tumor immune responses. Notably, “hot” tumors generally tend to respond more favorably to anti-PD-1/PD-L1 therapies [15]. Consequently, identifying biomarkers that differentiate between “cold” and “hot” tumors could offer a novel approach to enhance the predictive accuracy of immunotherapy outcomes.

To explore new biomarkers for immunotherapy, we systematically classified the TCGA-BLCA cohort using 29 immune cell and immune pathway-related gene sets, integrating this classification with the IMvigor210 immunotherapy cohort data to identify potential biomarkers. Our comprehensive analysis focusing on expression levels and prognostic significance led to the selection of Apolipoprotein L6 (APOL6) for further investigation. Subsequently, the diagnostic potential of APOL6 was corroborated in immunotherapy cohorts comprising BLCA, breast cancer (BRCA), and melanoma (SKCM)

patients. What’s more, we aim to investigate the underlying mechanism for the role of APOL6 in BLCA. Our findings provide APOL6 may emerge as a novel biomarker and promising immunotherapy target for BLCA and possibly other malignancies.

Method and material

Public data acquisition

The immunotherapy cohort’s RNA-seq data, including GSE176307 [16], GSE173839 [17], GSE194040 [18], and PRJEB23709 [19], as well as chemotherapy cohort data (GSE104580), were sourced from the Gene Expression Omnibus (GEO) (<https://www.ncbi.nlm.nih.gov/geo/>) or the Tumor Immune Dysfunction and Exclusion (TIDE) databases (<http://tide.dfci.harvard.edu/>). Additionally, the IMvigor210 cohort’s [20] clinical and gene expression data were obtained from the corresponding website (<http://research-pub.gene.com/IMvigor210/CoreBiologies/>). We acquired the pan-cancer standardized RNA-seq datasets and clinical information from the UCSC database (<https://xenabrowser.net/datapages/>). The abbreviations reference of TCGA cancer types are listed in Table 1.

From the Cistrome Cancer database (<http://cistrome.org/CistromeCancer/>), a substantial data collection of 318 tumor-related transcription factors (TFs) was acquired [21].

Single sample enrichment analysis and cluster analysis

The immune characteristics of each sample were comprehensively evaluated by ssGSEA algorithm that implementation provided by the “GSVA” R package [22] relying on 29 gene sets related to immune [23], encompassing immune cell types, functional pathways, and immune checkpoints. Every ssGSEA score x_i transformed into x_i' via deviation standardization, and subsequently, immune subtypes for BLCA patients were determined through cluster analysis. The t-distributed Stochastic Neighbor Embedding (tSNE) algorithm [24], implemented through the R package Rtsne, was used to verify the accuracy and discrimination of the subtypes in patients for BLCA.

Assessment of immune and stromal context and immune cell composition

Considering that bulk RNA-Seq data from tumor tissues encompass both tumor and normal cells, an assessment of the immune feature of the TME in each specimen was conducted. To gain a deeper understanding of the immunological context within each tumor sample, the ‘Estimate’ R package [25] was employed to evaluate the immunological characteristics of each TME sample. This software facilitated a detailed evaluation of the immune infiltrate, shedding light on the

Table 1 Table of abbreviations in the TCGA database

Abbreviation	Full name
ACC	adrenocortical carcinoma
BLCA	bladder urothelial carcinoma
BRCA	breast invasive carcinoma
CESC	cervical squamous cell carcinoma and endocervical adenocarcinoma
CHOL	cholangiocarcinoma
COAD	colon adenocarcinoma
DLBC	lymphoid neoplasm diffuse large B-cell lymphoma
ESCA	esophageal carcinoma
GBM	glioblastoma multiforme
HNSC	head and neck squamous cell carcinoma
KICH	kidney chromophobe carcinoma
KIRC	kidney renal clear cell carcinoma
KIRP	kidney renal papillary cell carcinoma
LGG	brain lower grade glioma
LIHC	liver hepatocellular carcinoma
LUAD	lung adenocarcinoma
LUSC	lung squamous cell carcinoma
MESO	mesothelioma
OV	ovarian serous cystadenocarcinoma
PAAD	pancreatic adenocarcinoma
PCPG	pheochromocytoma and paraganglioma
PRAD	prostate adenocarcinoma
READ	rectum adenocarcinoma
SARC	sarcoma
SKCM	skin cutaneous melanoma
STAD	stomach adenocarcinoma
TGCT	testicular germ cell tumor
THCA	thyroid carcinoma
THYM	thymoma
UCEC	uterine corpus endometrial carcinoma
UCS	uterine carcinosarcoma
UVM	uveal melanoma

diverse immune cell populations present and their potential influence on tumor progression. To further refine the immune cell components within the TME, CIBERSORT algorithm that implemented by Stanford [26] to comprehensively calculate the infiltration levels of tumor-infiltrating immune cells (TIICs) in each specimen using RNA sequencing data. Additionally, four other independent algorithms—EPIC [27], MCP [28], quanTIseq [29], and TIMER [30]—were utilized to validate the accuracy of the immuno-infiltration assessment in the TME.

Screening differential genes

We employed the limma R package to perform a differential expression analysis, aiming to identify genes exhibiting significant expression differences across distinct immune subtypes. Genes with a *P*-value less than 0.05 were designated as differentially expressed genes (DEGs), providing us with a set of potential targets for further exploration. The DESeq2 R package was employed to process the count data from the IMvigor210 cohort, with genes exhibiting a *P* value < 0.05 being designated as DEGs. Subsequently, common gene candidates between the TCGA-BLCA and IMvigor210 datasets were identified through Venn analysis.

Enrichment analysis and functional annotation

To explore the signaling pathways of intersecting candidates, Kyoto Encyclopedia of Genes and Genomes (KEGG) enrichment analyses were conducted through the clusterProfiler R package. The enriched terms with a *P* value < 0.05 were deemed significant, and the top 10 significant objects were retained. C5.all.v7.0 gene sets and Hallmark collections were downloaded from the Molecular Signatures Database (MSigDB) [31]. The top five upregulated biological processes and pathways were identified using Gene Set Enrichment Analysis (GSEA).

Estimating the immune landscape of the tumor microenvironment in BLCA

The substantial diversity of the TME is pivotal in impacting the effectiveness of tumor treatment. Immunological characteristics of the TME include the presence of immune modulators, activation of the tumor immune cycle, levels of immune cell penetration, and expression of immune checkpoints in BLCA. We assessed the expression of 150 immunomodulators, including MHC, receptors, chemokines, immunostimulators, and immunoinhibitors. The cancer immune cycle, fundamental to tumor immunotherapy, consists of seven steps: release of cancer antigens (Step 1), cancer antigen presentation (Step 2), priming and activation (Step 3), trafficking of immune cells to tumors (Step 4), recognition of cancer cells by T cells (Step 5), and killing of these cancer cells (Step 6) [32]. Moreover, effector molecules of TIICs were analyzed to further confirm the infiltration degree of immune cells in tumor tissues. The relevance of APOL6 to immunotherapy was evaluated through the following aspects: As reported previously, Immunophenoscore (IPS) were calculated to forecast the outcomes of immunotherapy interventions [33]. IPS values for BLCA patients were acquired from the Cancer Immunome Atlas (TCIA) website (<http://tcia.at/home/>). Next, we collocated Gene sets for anti-tumor immune-related biological

processes and tumor immunotherapy to calculate enrichment scores (Table 2). Furthermore, the level of immune checkpoints could reflect the efficacy of immunotherapy to some extent. Thus, common immune checkpoints were analyzed for their correlation with APOL6.

The complex and diverse nature of the tumor microenvironment (TME) significantly influences the success of cancer therapies. Key immunological characteristics of the TME, including the presence of immune modulators, tumor immune cycle activity, immune cell infiltration levels, and immune checkpoint expression, are particularly relevant in BLCA. The cancer immune cycle, consisting of seven stages (release of cancer antigens, antigen presentation, priming and activation, immune cell trafficking to tumors, T cell recognition of cancer cells, infiltration, and killing of cancer cells), serves as a framework for understanding tumor immunotherapy. We examined the effector molecules of TIICs to ascertain the level of immune cell infiltration into tumor tissues. To assess APOL6’s relevance in immunotherapy, we applied several analyses. First, we used the Immunophenoscore (IPS), a predictive tool for immunotherapy outcomes, obtained from The Cancer Immunome Atlas (TCIA) website. Next, we employed gene sets associated with anti-tumor immune processes and immunotherapy to determine enrichment scores (Table 2). Since immune checkpoint levels can indicate immunotherapy effectiveness, we investigated the correlation between APOL6 and common immune checkpoints.

Construction of interaction networks

We combined Hawk Dock [34], ClusPro2.0 [35], and AlphaFold2 [36] to determine Ferroptosis-related proteins’ potential to interact with APOL6. Using the

Prime module, each ligand molecule’s relative binding free energy was calculated via the MMGBSA method. This calculation was instrumental in assessing the binding affinity between the ligands and the receptor. The MMGBSA Prime module also determined the energies for the unbound receptor, unbound ligand, and receptor-ligand complex. All settings are default [37].

The process is as follows:

1. Access the protein structure by prediction in AF2.
2. Docking the protein.
3. Analysis of protein metrics.

To explore the association between tumor-related transcription factors and APOL6 in BLCA, we obtained transcription factors data from the Cistrome Cancer database (<http://cistrome.org/CistromeCancer/>) and constructed a co-expression network that was established relying on the TCGA BLCA dataset. The filter condition for correlation coefficients was set at $cor > 0.35$ and $P < 0.001$. To validate key upstream regulatory genes, we constructed a transcription factor (TF)-gene-interactions network using the online tool NetworkAnalyst [38].

Antibodies, reagents as well as plasmids

The APOL6 overexpression and ACSL4 siRNA plasmids were provided by Gene Pharma (Shanghai, China). The antibodies were used as follows. APOL6 was from Affinity company (DF9219), ACSL4 was from Proteintech (22401), and ACTB was from Sigma (A5316). Fludara, the inhibitor of STAT1 was from APEXBIO (A8317).

Table 2 Detailed information of immunotherapy-related gene signatures

Pathway	Reference	Gene markers
IFN-γ signature	PMID: 28650338	TIGIT, CD27, CD8A, PDCD1LG2, LAG3, CD274, CXCR6, CMKLR1, NKG7, CCL5, PSMB10, IDO1, CXCL9, HLA-DQA1, CD276, STAT1, HLA-DRB1, HLA-E
APM signal	PMID: 31563503	B2M, HLA-A, HLA-B, HLA-C, TAP1, TAP2
EGFR ligands	PMID: 31563503	EGFR, AREG, AREGB, EREG, HBEGF, TGFA
WNT/β-catenin network	PMID: 27197067	CTNNB1, TFF1, HAPLN1, IHH, WNT7B, BMP7, SEMA5A, SCN5A, ERBB3, TSPAN8, EPCAM, TH, GPX2, GAD1, HSD17B2, KRT7, NOX1, CYB5A, CYP4F12, ID4, SIM2, MECOM, MSX2, KLF5, SMAD6, POU5F1, FOXQ1, GATA2, GATA3, EMX2
Hypoxia	PMID: 31563503	CAV1, COL5A1, ITGA5, P4HA2, SLC16A1, TGFB1, DPYSL2, SRPX, TRAM2, SYDE1, LRP1, PDLIM2, SAV1, AHNK2, CAD, CYP1B1, DAAM1, DSC2, SLC2A3, FUT11, GLG1, GULP1, LDLR, THBS4
FGFR3-coexpressed genes	PMID: 31563503	FGFR3, TP63, IRS1, SEMA4B, PTPN13, TMPRSS4
PPARG network	PMID: 27197067	PPARG, IGF1BP3, GDF15, MYH14, IHH, OCLN, AQP3, SCNN1G, PLIN5, KRT19, GPT, CYP4B1, UGT1A7, DGAT2, KRT20, SNCG, GSTA1, ACADL, BDH1, HMGC52, LIPESNCG, GSTA1, ACADL, BDH1, HMGC52, LIPES
IDH1	PMID: 29326431	IDH1
KDM6B	PMID: 26503055	KDM6B
VEGFA	PMID: 24793239	VEGFA

Cell culture and transfection

T24 cells, obtained from the Cell Bank of Type Culture Collection of the Chinese Academy of Sciences, were cultured in DMEM medium supplemented with 10% fetal bovine serum (FBS) and 1% penicillin/streptomycin at 37°C under 5% CO₂ in a humidified cell incubator. When cultured to 70% confluence, the cells were transfected with APOL6 plasmid or siRNA against human ACSL4 for 48 h.

Measurement of lipid peroxidation

T24 cells were incubated with the oxidation-sensitive probe C11-BODIPY581/591 (Thermo, D3861) for 20 min. Following staining the nucleus with DAPI, the lipid peroxidation was observed and the images were captured by the fluorescence microscope.

Detection of free iron levels

T24 cells were incubated with the FerroOrange (1 μmol/L) probe which was purchased from DOJINDO (F374) for 30 min. The nuclei were stained with DAPI, followed by observation under the fluorescence microscope.

IP and immunoblotting analysis

We conducted IP following a previously described protocol [39]. Initially, cells were lysed in a lysis buffer for a duration of 30 min on ice. Subsequently, the lysates underwent centrifugation at 15,000 g for 15 min, with the resulting supernatant being transferred to a pre-chilled microcentrifuge tube. Following quantification of the protein concentration utilizing the BCA Protein Assay Kit (Beyotime, China), approximately 10% of the supernatant was reserved for Western analysis as inputs. A total of 1,500 μg of protein was then subjected to overnight incubation with specified antibodies, followed by a 2-h incubation with protein A- or protein G-agarose beads (Beyotime, China). The IP beads underwent five washes with lysis buffer prior to immunoblotting analysis. The protein was subsequently separated using sodium dodecyl sulfate-polyacrylamide gel electrophoresis (SDS-PAGE) with varying concentrations of 10% and 15%, and then transferred onto polyvinylidene fluoride membranes (Millipore, USA). Following a 2-h block with 5% skimmed milk dissolved in TBST, the membranes were exposed to primary antibody overnight at 4°C. Subsequent washing was followed by incubation with HRP-conjugated secondary antibodies for 1 h, and the results were ultimately visualized using the ECL western blotting detection system (Millipore, USA).

Statistical analysis

All statistical analyses and figure presentations were conducted based on the R language. Data were displayed

as mean ± standard deviations (SDs). The distinction between the two groups was evaluated using Student's t-test or the non-parametric Wilcoxon test. In cases of comparisons involving multiple groups, the Kruskal-Wallis test was employed to determine statistical differences. Moreover, the Pearson test was utilized for analyzing correlations between two variables. The prognostic significance of categorical variables was ascertained using log-rank tests and Cox regression analysis, while survival curves were derived through the Kaplan-Meier method. Furthermore, the purpose of Receiver-operating characteristic (ROC) analysis was to gauge the specificity and sensitivity of potential molecules, utilizing the area under the ROC curve (AUC) to evaluate the predictive accuracy of biomarkers. Every statistical test was two-sided, with a *P*-value < 0.05 regarded statistically significant, denoted as **P* < 0.05; ***P* < 0.01; ****P* < 0.001.

Result

Identification and validation of the immunological correlation in two subtypes of BLCA

The schematic diagram of the current study is showed in Fig. 1. To conduct a comprehensive assessment of the immunological characteristics in BLCA, we evaluated 29 immune-related pathways in the TCGA-BLCA cohort. By applying ssGSEA scores and conducting a clustering analysis, the BLCA cohort was categorized into two immune subtypes: Immunity_H (High) and Immunity_L (Low) (Figure S1A, B). The tSNE algorithm was subsequently utilized to validate the clustering of immune levels in BLCA patients, producing consistent results in classification (Figure S1C).

Further validation of the immunological relevance of these subtypes was performed using the ESTIMATE algorithm. Higher scores were observed in the Immunity_H subtype, while the Immunity_L group exhibited lower levels of EstimateScore, ImmuneScore, and StromalScore (Figure S1D). The degrees of immune cell infiltration between these subtypes were assessed by the CIBERSORT algorithm. We observed significant differences in the infiltration levels of CD8+ T cells, naïve CD4+ T cells, activated memory CD4+ T cells, M0 macrophages, eosinophils, and neutrophils. This analysis revealed that the Immunity_H subtype exhibited elevated levels of immune infiltration, especially in CD8+ T cells (Figure S1E), potentially improving the response to immunotherapy. Overall, these findings imply that the immunophenotyping of BLCA patients was effectively accomplished.

Identification of candidates for immunotherapy in BLCA

In the pursuit of discovering new biomarkers indicative of immunotherapy effectiveness, we sourced data on

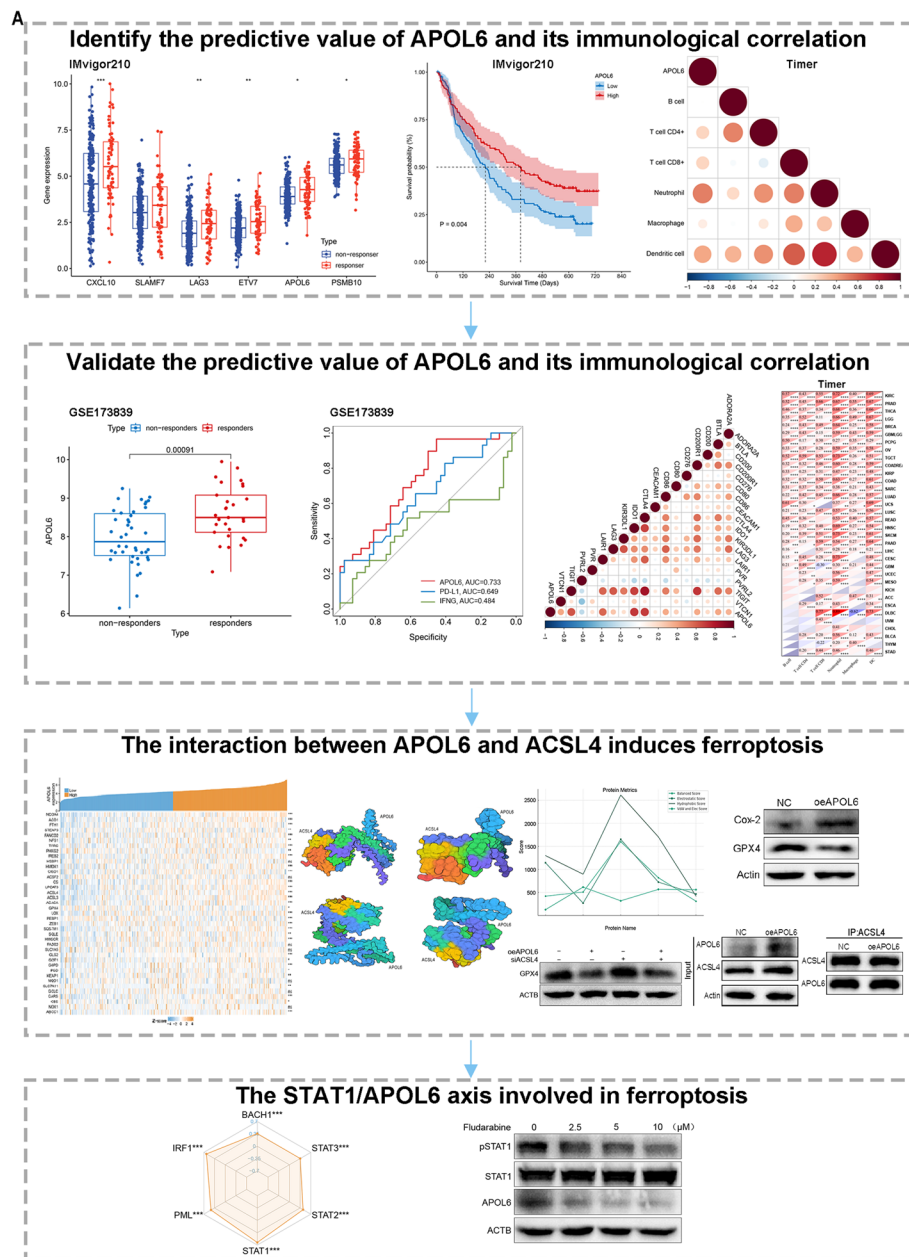


Fig. 1 Schematic diagram of the current study. The main results of this work consist of four parts

IMvigor210 from relevant websites. We analyzed DEGs with a significance threshold of $P < 0.01$. This included a total of 2760 up-regulated DEGs in TCGA immunity-High subtypes (Figure S1F), 1467 DEGs in responders (CR/PR) in the IMvigor210 dataset (Figure S1G), and 894 DEGs in survivors in IMvigor210 (Figure S1H). Subsequently, through Venn analysis, we identified 31 common candidate molecules (Figure S1I). They were enriched in pathways related to immunity, including the Toll-like receptor signaling pathway, NOD-like receptor signaling pathway,

Chemokine signaling pathway, Cytokine-cytokine receptor interaction, Antigen processing and presentation, and Natural cell-mediated cytotoxicity (Figure S1J). Overall, these findings suggest that the 31 potential candidate molecules in BLCA are related to immunotherapy.

Expression, and prognostic values of potential biomarkers in BLCA

Next, 31 potential biomolecules were analyzed for prognostic significance in BLCA (Figure S2). Genes exhibiting

a P -value < 0.05 and a hazard ratio (HR) < 1 , indicative of improved prognosis, have been identified. These include APOL6, CXCL10, ETV7, LAG3, PSMB10, and SLAMF7, all associated with improved prognosis in BLCA (Fig. 2A). Subsequently, we analyzed the expression levels of these prognostic genes with statistical significance in the IMvigor210 and TCGA-BLCA datasets, and validated

their expression in the GSE176307 dataset. In the TCGA dataset, the expression of CXCL10, ETV7, and APOL6 was notably elevated in tumor tissues as opposed to para-tumor tissues (Fig. 2B). Regarding the IMvigor210 cohort, the levels of CXCL10, LAG3, ETV7, APOL6, and PSMB10 were significantly upregulated in the immunotherapy-responsive population (Fig. 2C). Notably,

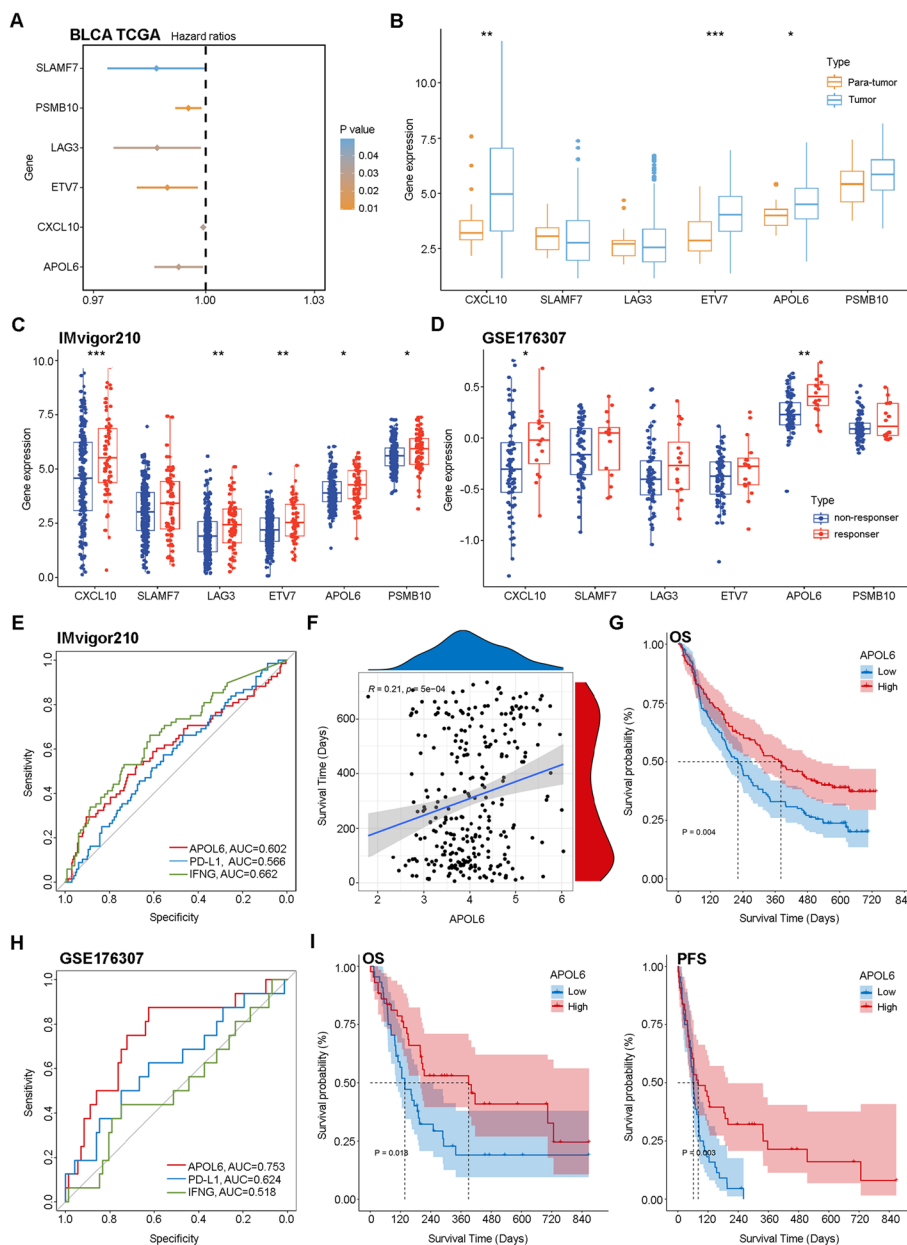


Fig. 2 Patterns of expression and the predictive significance of potential biomarkers. **A** Prognostic values of 6 candidates (P value < 0.05) in the TCGA-BLCA cohort. **B** Expression levels of 6 candidates between tumor and para-tumor in TCGA-BLCA cohort. **C** Expression of 6 candidates between responder and non-responder in IMvigor210 cohort. **D** Expression levels of 6 candidates between responder and non-responder verified in the GSE176307 cohort. **E** Comparison of the predictive significance of APOL6, PD-L1, IFN- γ in IMvigor210 cohort. **F** Correlation between APOL6 expression and survival time (OS) in IMvigor210 cohort. **G** Prognostic values of APOL6 in terms of OS. **H** Evaluation of the predictive significance of APOL6, PD-L1, IFN- γ in verification set of GSE176307. **I** Prognostic values of APOL6 regarding OS and PFS confirmed in the GSE176307 cohort

APOL6 and CXCL10 levels were significantly elevated in the tumor samples with the response group in the GSE176307 cohort (Fig. 2D). Therefore, our study found that APOL6 and CXCL10 exhibit elevated expression levels in the immunotherapy-responsive subgroup, demonstrate heightened expression within tumor tissues, and offer favorable prognostic implications. Patients with elevated APOL6 expression, as opposed to CXCL10, exhibit a reduced risk of disease progression in BLCA, thereby warranting further research on APOL6. The predictive value of APOL6, PD-L1, and IFN- γ in the IMvigor210 immune cohort was compared. While the capacity of APOL6 to differentiate treatment responses was moderate (AUC=0.602), it still surpassed that of PD-L1 (AUC=0.566) (Fig. 2E), a finding corroborated in the GSE176307 dataset, where APOL6 (AUC=0.753) demonstrated superior discriminative ability for treatment response compared to PD-L1 (AUC=0.624) (Fig. 2H). The immunotherapy cohort was categorized into groups with low and high APOL6 expression, determined by the median level of expression. It was observed that APOL6 expression is positively correlated with immunotherapy survival time, with patients exhibiting high APOL6 expression having longer overall survival (OS) (Fig. 2F, G). Validation through the GSE176307 dataset confirmed that APOL6 expression levels positively correlate with both overall survival (OS) and progression-free survival (PFS) (Fig. 2I), reinforcing the potential of APOL6 expression as an indicative biomarker for immunotherapy in BLCA.

APOL6 recognized as a potential biomarker for forecasting the outcome of immunotherapy in BLCA

To corroborate the prognostic significance of APOL6 in immunotherapy for BLCA, we explored the association between APOL6 and the TME effect using the IMvigor210 and GSE176307 datasets. The expression of APOL6 showed a notable correlation with the expression levels of PD-L1 in both immune cell (IC) and tumor cell (TC) scores (Fig. 3A, B). Additionally, higher levels of APOL6 expression were associated with more 'inflamed' tumor tissues (Fig. 3C). Furthermore, according to IMvigor210 and GSE176307 cohorts, APOL6 expression levels were found to be positively correlated with neoantigen burden and tumor mutation load in the TME (Fig. 3D-F). Our subsequent analysis focused on the link between APOL6 expression levels and common immune checkpoints, encompassing PD1, PD-L1, cytotoxic T lymphocyte antigen 4 (CTLA4), cluster of differentiation 86 (CD86), hepatitis A virus cellular receptor 2 (HAVCR2), lymphocyte activation gene-3 (LAG-3), and T-cell immunoglobulin and ITIM domain (TIGIT). The levels of APOL6 expression demonstrated

a positive correlation with the levels of common immune checkpoints within the IMvigor210 cohort, and comparable findings were observed in the GSE176307 cohort (Fig. 3G). As previously reported, the IFN- γ signature, APM signal, and Hypoxia show a positive correlation with responses to immunotherapy [40]. In contrast, FGFR3-coexpressed genes, PPAR- γ , VEGFA pathway, and the WNT/ β -catenin signaling pathways indicate a 'cold' immune microenvironment [41]. The association between APOL6 expression and enrichment scores relevant to immunotherapy was evaluated, revealing a positive association with the IFN- γ signature, APM signal, and Hypoxia for APOL6. Conversely, there is a negative association between APOL6 and FGFR3-coexpressed genes, IDH1, PPAR- γ , WNT/ β -catenin, and the VEGFA pathway (Fig. 3H). These findings imply that patients exhibiting higher APOL6 expression may potentially gain advantages from immunotherapy.

Immunological correlations of APOL6 in BLCA

Given the significant correlation between APOL6 and the efficacy of tumor immunotherapy, the GSEA was performed on cohorts with high and low APOL6 levels to further investigate the function of APOL6 and the pathways involved. In the C2 collection as defined by MSigDB, differential gene functions were primarily enriched in immune biological processes, including the interferon gamma-mediated signaling pathway, MHC protein complex, peptide antigen binding, response to interferon gamma, and response to type I interferon in GO gene sets of the APOL6 high expression cohort (Fig. 4A). Similarly, in both HALLMARK and KEGG gene sets, enhanced immune activation was observed in the APOL6 high expression cohort (Fig. 4B, Figure S3A). To further decipher the relationship between APOL6 and the TME in BLCA, we conducted immune scoring on TCGA samples. It was observed that APOL6 expression had a positive correlation with the Stromal score, immune score, and ESTIMATE score as expected, yet exhibited a negative correlation with tumor purity (Fig. 4C). Additionally, APOL6 was significantly associated with the infiltration levels of tumor-infiltrating immune cells (TIICs); heightened expression of APOL6 correlates with an augmented presence of activated CD8⁺ T cells, M1 macrophages, and dendritic cells, while Treg infiltration diminishes (Fig. 4D). The above results indicate that APOL6 has a positive association with the infiltration of pro-inflammatory immune cells and a negative association with the infiltration of immune-suppressive cells (Figure S3B and C). Specifically, high infiltration of CD8⁺ T lymphocytes favors immunotherapy checkpoint treatment of tumors, while a decrease in Treg cells can alleviate

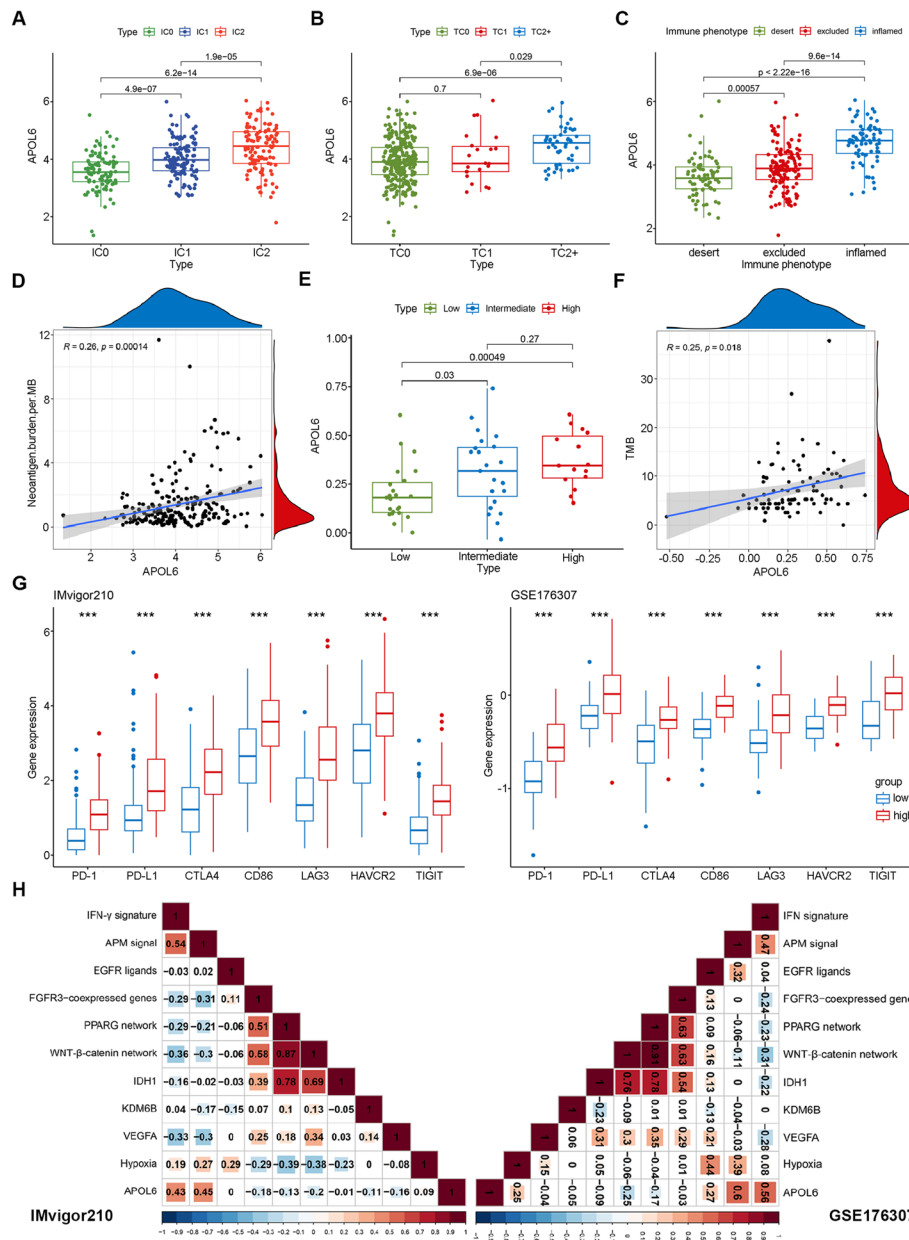


Fig. 3 Correlation between APOL6 and immune phenotype in BLCA immunotherapy cohorts. **A** APOL6 levels across tumors with various PD-L1 IC score within the IMvigor210 cohort. **B** APOL6 levels across tumors with various PD-L1 TC score within the IMvigor210 cohort. **C** Levels of APOL6 expression across tumors with varied immuno-subtypes in IMvigor210 cohort. **D** The relationship between APOL6 expression and neoantigen burden in the IMvigor210 cohort was analyzed by Pearson correlation analysis for significance. **E** APOL6 expression across tumors exhibiting various TMB levels verified in GSE176307. **F** The association between APOL6 expression and TMB levels was analyzed by Pearson correlation analysis for significance in GSE176307. **G** Differences in levels of immune-related targets in low and high APOL6 groups in the IMvigor210 cohort and verified in the GSE176307 cohort. **H** The association between APOL6 and immune-related pathways in two immunotherapy cohorts

tumor immune suppression and enhance the efficacy of tumor-eliminating cells like CD8⁺ T cells (Fig. 4E). In summary, APOL6 is strongly related to tumor immune infiltration, with the significant positive relationship between APOL6 expression levels and the infiltration of activated immune cells being of particular importance,

potentially aiding in the improvement of immune checkpoint therapy efficacy.

The significance of APOL6 within the inflamed TME in BLCA
The TME comprises a variety of elements including tumor cells, immune cells, stromal elements,

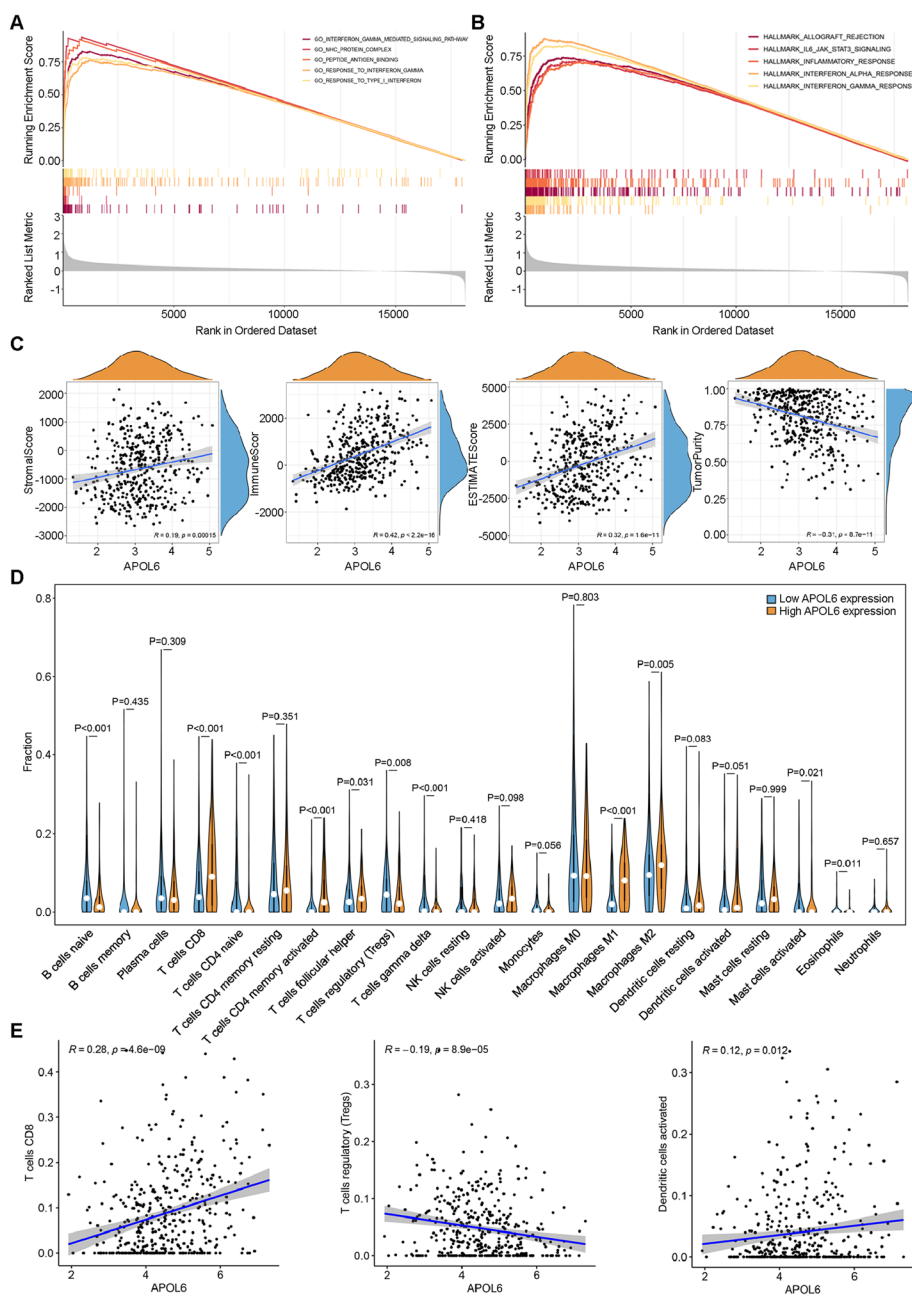


Fig. 4 Immuno-correlations of APOL6 in BLCA. **A** Enriched gene sets in G5 collection, the GO gene sets, by sample of elevated APOL6 expression. Each line symbolizes a specific gene set, distinguished by a different color. Only the top 5 gene sets showed. **B** Enriched gene sets in HALLMARK collection by samples of high APOL6 expression. **C** Correlation between APOL6 and TumorPurity, Stroma score, Immune Score, ESTIMATE Score. **D** TIICs abundance in the high and low APOL6 groups estimated by the CIBERSOR method in BLCA. **E** Correlation between APOL6 and dendritic cells activated, T cells CD8, Tregs

chemokines, and cytokines, and is intimately associated with tumor occurrence and progression. Given the relationship between APOL6 and the immune micro-environment, along with immunotherapy responsiveness, we further explored the immuno-relationship of APOL6 in the TCGA -BLCA cohort. APOL6 was

identified as being positively correlated with a wide range of immunomodulators, including chemokines, immunoinhibitors, immunostimulators, MHC molecules, and receptors (Figure S4A). Immunomodulators are pivotal in initiating the cycle of cancer immunity. We assessed the association between APOL6 and each

step of the cancer-immunity cycle, and found that high APOL6 expression facilitated immune cell infiltration, recognition, and killing of tumor cells, particularly tumor antigen presentation, as well as the attraction and activation of CD8⁺ T cells, Th1 cells, and natural killer cells (Figure S4B). The enhanced activities of these steps may lead to increased infiltration levels of effector TIICs in the TME. As expected, there is a positive connection between APOL6 and the majority of TIIC abundance (Figure S4C). Additional analysis indicated that increased APOL6 expression correlated with enhanced TIICs (Figure S7A). Similarly, effector genes of these TIICs showed a marked increase in the group exhibiting high APOL6 expression (Figure S4D). Overall, there is a strong correlation between APOL6 and the inflamed TME, positioning it as an indicative marker of immuno-hot tumors in BLCA.

APOL6 predicts immune phenotype in BLCA

IPS can indicate immunotherapy response, and our findings revealed that patients with elevated APOL6 expression exhibited notably high IPS (Figure S5A). APOL6 demonstrated a positive correlation with common immune checkpoints, including TIGIT, CTLA4, and LAG3, among others (Figure S5B, D). Additionally, enrichment scores related to immunotherapy, like the IFN- γ signature and APM signal, showed an increase in the group with elevated APOL6 expression. Conversely, APOL6 levels were negatively associated with PPAR- γ and WNT- β -catenin signaling pathways (Figure S5C). In conclusion, patients exhibiting higher APOL6 levels potentially demonstrate enhanced sensitivity to immunotherapy in BLCA.

Exploring the immunological role of APOL6 in pan-cancer analysis

Given the link between APOL6 and immuno-hot tumors, and its ability to foresee an improved response to immunotherapy, we further investigated the relationship between APOL6 and inflamed TME through a comprehensive pan-cancer analysis of the TCGA dataset. The analysis revealed that APOL6 had a positive correlation with immunomodulators, including chemokines, receptors, major histocompatibility complex (MHC), immunoinhibitors, and immunostimulators, across almost all cancer types (Figure S6A). Moreover, in most tumors, higher APOL6 expression levels were often associated with lower tumor purity and higher levels of tumor-infiltrating lymphocytes (TILs) (Figure S6B, C). Taken together, high APOL6 expression indicates an inflamed TME in various tumor types.

APOL6 predicts the responses to both immunotherapy and chemotherapy across various cancer types

Based on the above results, it was found that APOL6 has a strong association with the infiltration of immune cells in BLCA, BRCA, SKCM, and liver cancer. Moreover, higher APOL6 expression levels correlated with more active tumor immune microenvironments, predominantly characterized by CD8⁺ T cell infiltration, which may enhance the efficacy of immunotherapy and chemotherapy in patients. Additional databases were utilized to further explore the role of APOL6 in predicting immunotherapy and chemotherapy outcomes in human cancers. A total of four validation cohorts were employed, including GSE173839, GSE194040, PRJEB23709, and GSE104580. Interestingly, APOL6 expression was significantly upregulated in the treatment-responsive population across these cohorts (Fig. 5A, E, I, Figure S7B). Additionally, in the GSE173839 and PRJEB23709 datasets, APOL6 demonstrated more effective discrimination in immunotherapy outcomes compared to PD-L1. Although IFN- γ also showed satisfactory discriminative ability, its stability was lacking (Fig. 5B, F, J). Also, APOL6 showed a positive association with the majority of immune checkpoints in these cohorts, including CTLA4, PDL1, PD1, LAG3, TIGIT, and others (Fig. 5C, D, G, H, K, L).

Exploring the correlation between APOL6 and ferroptosis

Given the close relationship between APOL6 expression and patient sensitivity to immunotherapy and chemotherapy across various cancer types, it is imperative to explore the underlying mechanisms. We discovered that APOL6 expression is significantly correlated with ferroptosis markers (Table 3): elevated levels of APOL6 are associated with reduced levels of glutathione peroxidase 4 (GPX4) and increased levels of ACSL4 (Fig. 6A, B). Furthermore, we overexpressed APOL6 in T24 cells and found the expression of Cox-2 increased while the expression of GPX4 decreased, indicating that APOL6 promotes ferroptosis (Fig. 6C). Additionally, we also found overexpression of APOL6 obviously induced lipid peroxidation (Fig. 6D) and increased free iron levels (Fig. 6E). Taken together, these data suggested that APOL6 contributed to ferroptosis.

The interaction between APOL6 and ACSL4 induces ferroptosis in BLCA

We gathered five ferroptosis-related proteins to interact with APOL6 (Fig. 7A-D). As Fig. 7E presented, the ACSL4 represents potential hydrophilic-based interaction with APOL6. The other protein candidates' scores were all lower than ACSL4. Therefore, we select the

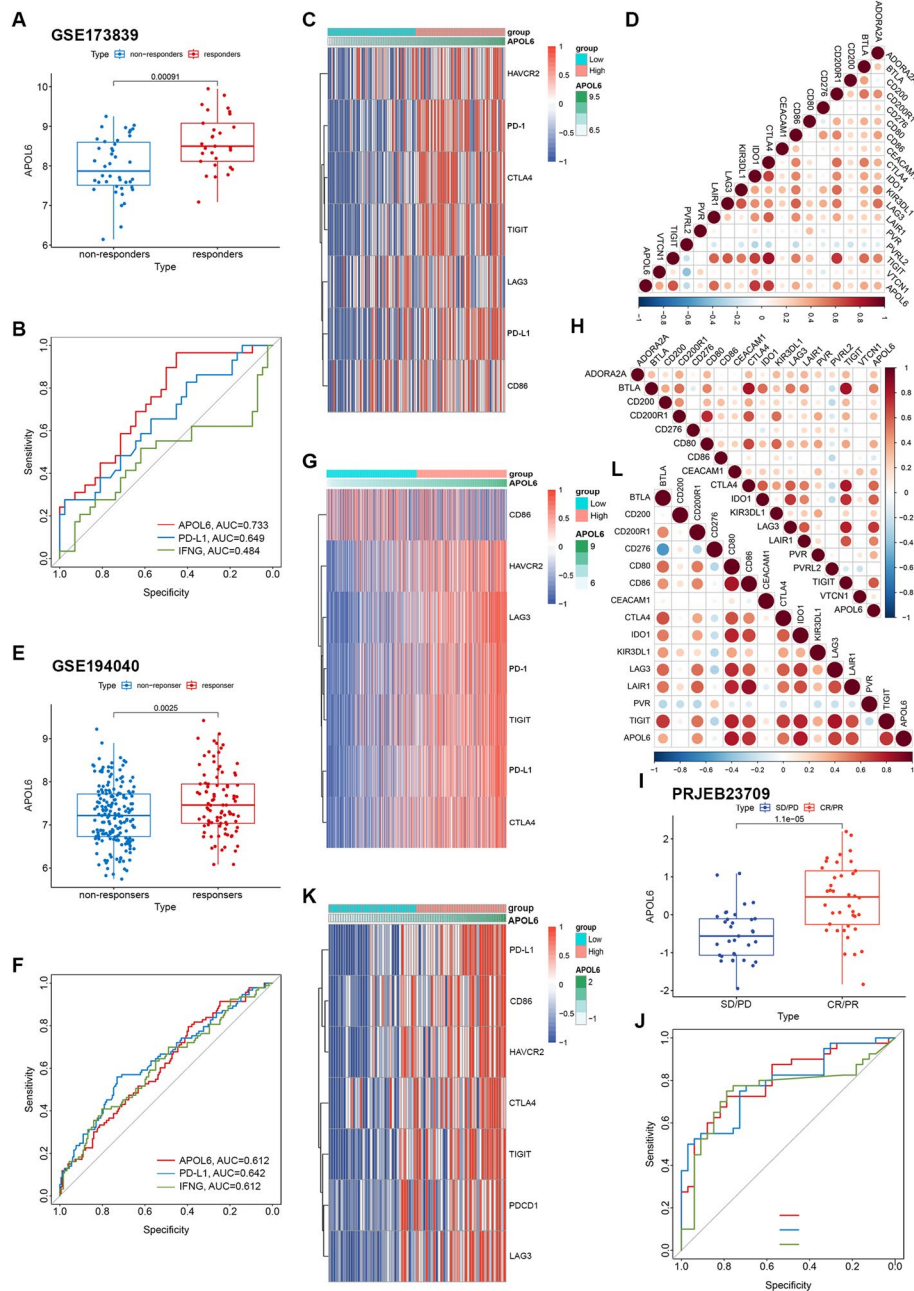


Fig. 5 Expression levels and immunotherapy correlation of APOL6 in BRCA and SKCM immunotherapy cohorts. **A** and **E** Differential expression of APOL6 in samples from responders and non-responders within GSE173839 and GSE194040 cohorts. **B** and **F** Evaluation of predictive values of APOL6, PD-L1, IFN- γ in BRCA immunotherapy cohorts. **C** and **G** Heatmap showing the correlation between APOL6 and immune-related targets in BRCA cohorts. **D** and **H** Correlation between APOL6 expression and common inhibitory immune checkpoints in BRCA. Significance was determined using Pearson correlation analysis. **I** Differential expression of APOL6 in samples from responders and non-responders in SKCM immunotherapy cohort. **J** Comparison of predictive values of APOL6, PD-L1, IFN- γ in SKCM. **K** Heatmap displaying the correlation between APOL6 and immune-related targets in SKCM cohorts. **L** Correlation between APOL6 expression and common inhibitory immune checkpoints in SKCM. Significance was determined using Pearson correlation analysis

ACSL4 as the potential protein interacting with APOL6. IP result further confirmed that there was interaction between APOL6 and ACSL4 (Fig. 7F). To further confirm

ferroptosis in T24 cells was mediated by interaction between APOL6 and ACSL4, we overexpressed APOL6 and silenced ACSL4 in T24 cells, western blot result

Table 3 Ferroptosis-related genes as identified in scientific publications

NCOA4 ACO1 FTH1 STEAP3 FANCD2 NFS1 TFRG PHKG2 IREB2 HSBP1 HMOX1
 C1SD1/mitoNEET.
 ACSF2 CS (citrate synthase) LPCAT3 ACSL4 ACSL3 ACACA GPX4 AKR1C LOX
 PEBP1 ZEB1 SQS/FDFT1 SQLE HMGCR FADS2
 SLC1A5 GLS2 GOT1 G6PD PGD
 NRF2 KEAP1 HMOX1 NQO1 SLC7A11 GCLC CARS CBS NOX1 ABCB1/MRP

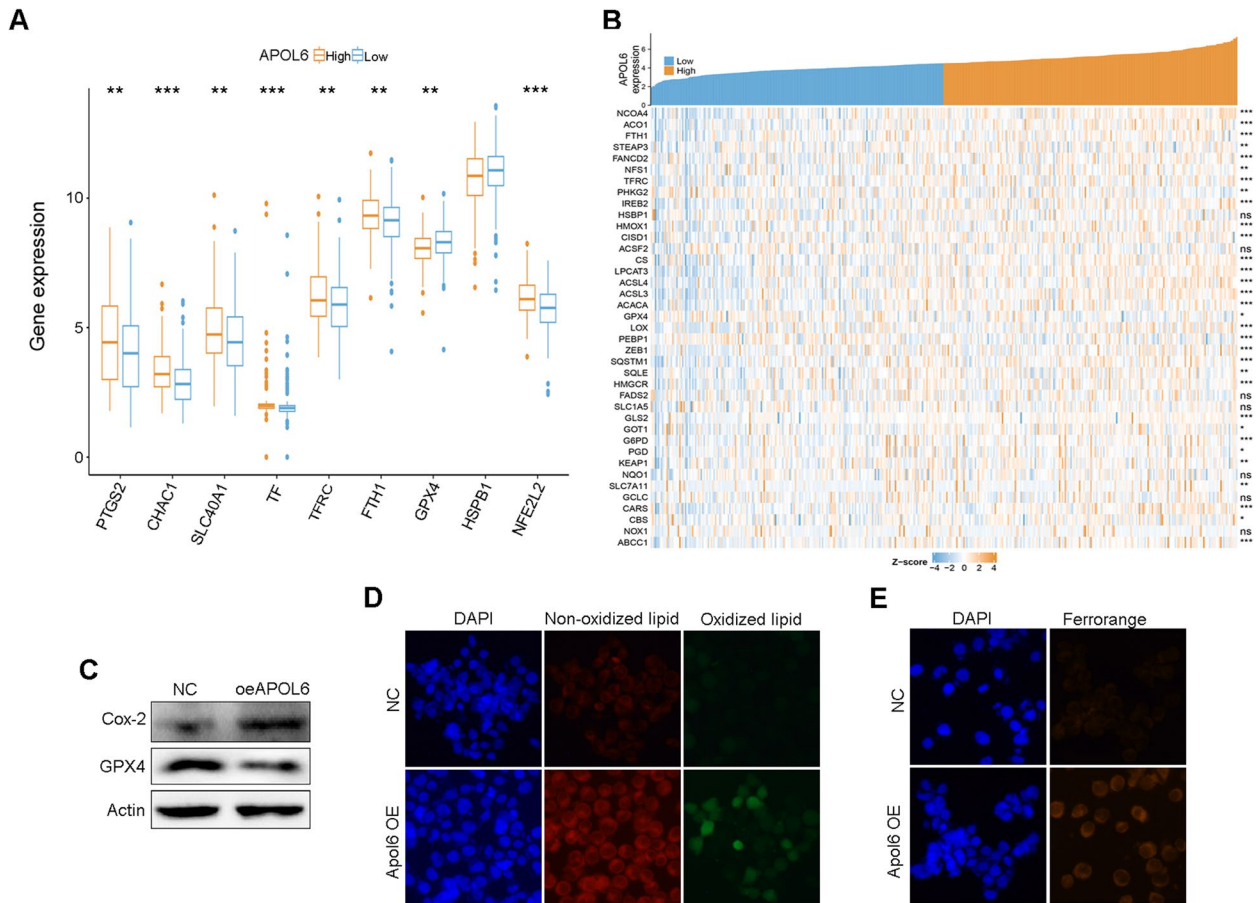


Fig. 6 APOL6 as a key regulatory factor in inducing ferroptosis in BLCA. **A** and **B** Relation between APOL6 and ferroptosis-related markers. **C** Levels of the Cox-2 and GPX4 protein in T24 cells following transfected with APOL6. **D** Lipid peroxidation in T24 cells was detected by C11-BODIPY581/591 probe. **E** T24 cells were transfected with APOL6, followed by detection with FerroOrange probe

showed that reduced GPX4 level induced by APOL6 was reversed by silencing of ACSL4 (Fig. 8A). Besides, Fig. 8B and C also revealed that ACSL4 knockdown significantly alleviated lipid peroxidation and free iron levels caused by overexpression of APOL6. Taken together, these findings demonstrated APOL6 mediated ferroptosis by interacting with ACSL4 in BLCA.

The STAT1/APOL6 axis induces ferroptosis in BLCA

We utilized the Cistrome database to analyze potential upstream transcription factors of APOL6. The radar

chart displayed transcription factors significantly associated with APOL6, among which STAT1 showed the strongest correlation (Fig. 9A). Additionally, the NetworkAnalyst tool was used to validate the predicted interacting transcription factors, with results indicating the presence of STAT1, suggesting that APOL6 expression may be regulated by STAT1 (Figure S7C). As a result, to further verify that APOL6 was regulated by STAT1, Fludarabine, an inhibitor of STAT1 was used. As shown in Fig. 8B, Fludarabine significantly suppressed the expression of APOL6, in a dose-dependent manner,

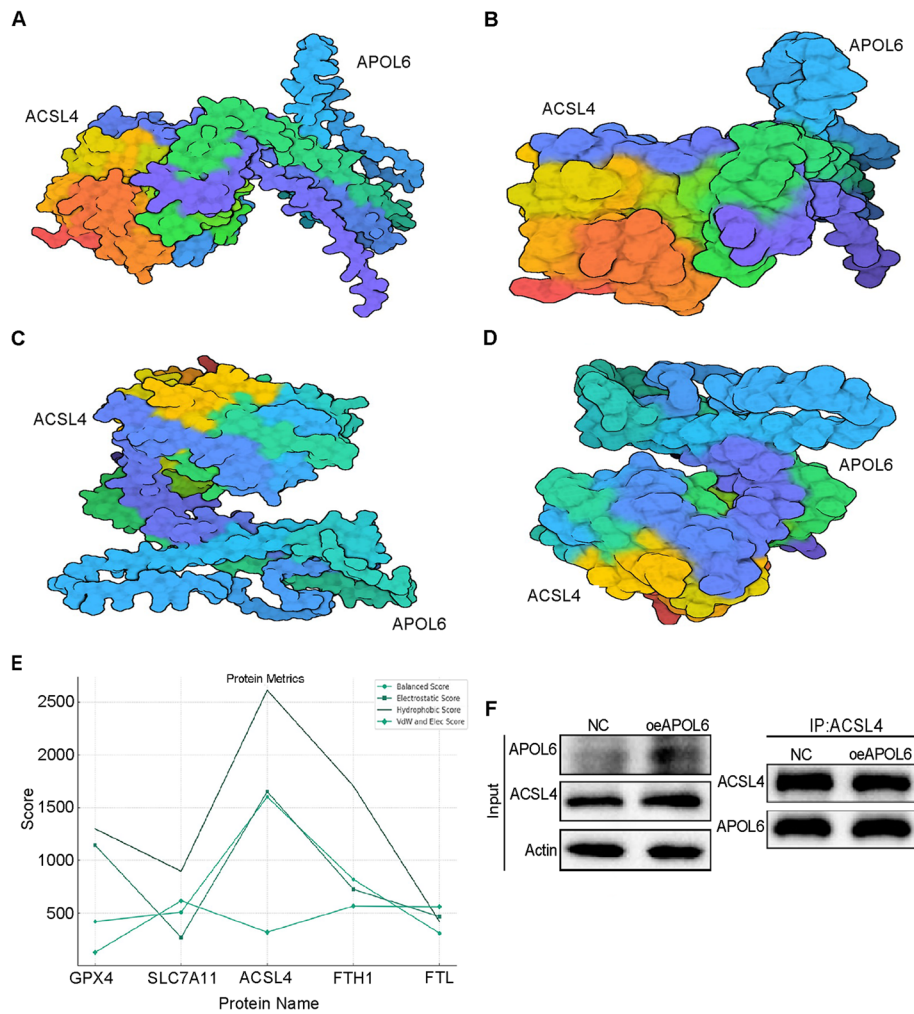


Fig. 7 Interaction between APOL6 and ACSL4 in BLCA. **A** The interaction of APOL6 contact surface with ACSL4 (Protein structure generated by AlphaFold 2). **B** The potential chain interaction between APOL6 and ACSL4. **C** The SAS interaction plot between APOL6 and ACSL4 (Protein structure generated by AlphaFold 2). **D** The SAS potential chains interaction between APOL6 and ACSL4 (Protein structure generated by AlphaFold 2). **E** The protein metric to determine the Ferroptosis-related proteins interact with APOL6. **F** The interaction of APOL6 with ACSL4 was detected by IP analysis

accompanied by reduced lipid peroxidation (Fig. 9C) and free iron levels (Fig. 9D).

Discussion

At present, traditional surgery, chemotherapy and radiotherapy cannot meet the current demand for BLCA treatment. Immunotherapy is becoming increasingly popular. Finding more effective and precise immunotherapy targets is particularly urgent.

APOL6, a pro-apoptotic BH3-only protein, is closely associated with apoptosis and autophagy. Reports indicate that the up-regulation of APOL6 induces mitochondria-mediated apoptosis in colorectal cancer [42]. Cancers are marked by the proliferation of malignant

cells and altered immune reactions. Being a downstream target of several pro-inflammatory signaling molecules, APOL6 holds a vital position in the immune system [43]. IFN- γ slows tumor growth and exerts pleiotropic impacts on anti-tumor immunity relying on the TME [44]. Interestingly, IFN- γ treatments significantly enhance the expression of APOL6 [45]. In this study, we discovered and demonstrated that APOL6 is an essential biomarker for evaluating the effectiveness and predicting outcomes of immunotherapy in BLCA. We suggest that enhancing APOL6 expression could be beneficial in immunotherapeutic strategies for BLCA. Drawing on the relationship between APOL6 and the features of the TME, we further confirmed that APOL6 shapes an inflamed tumor

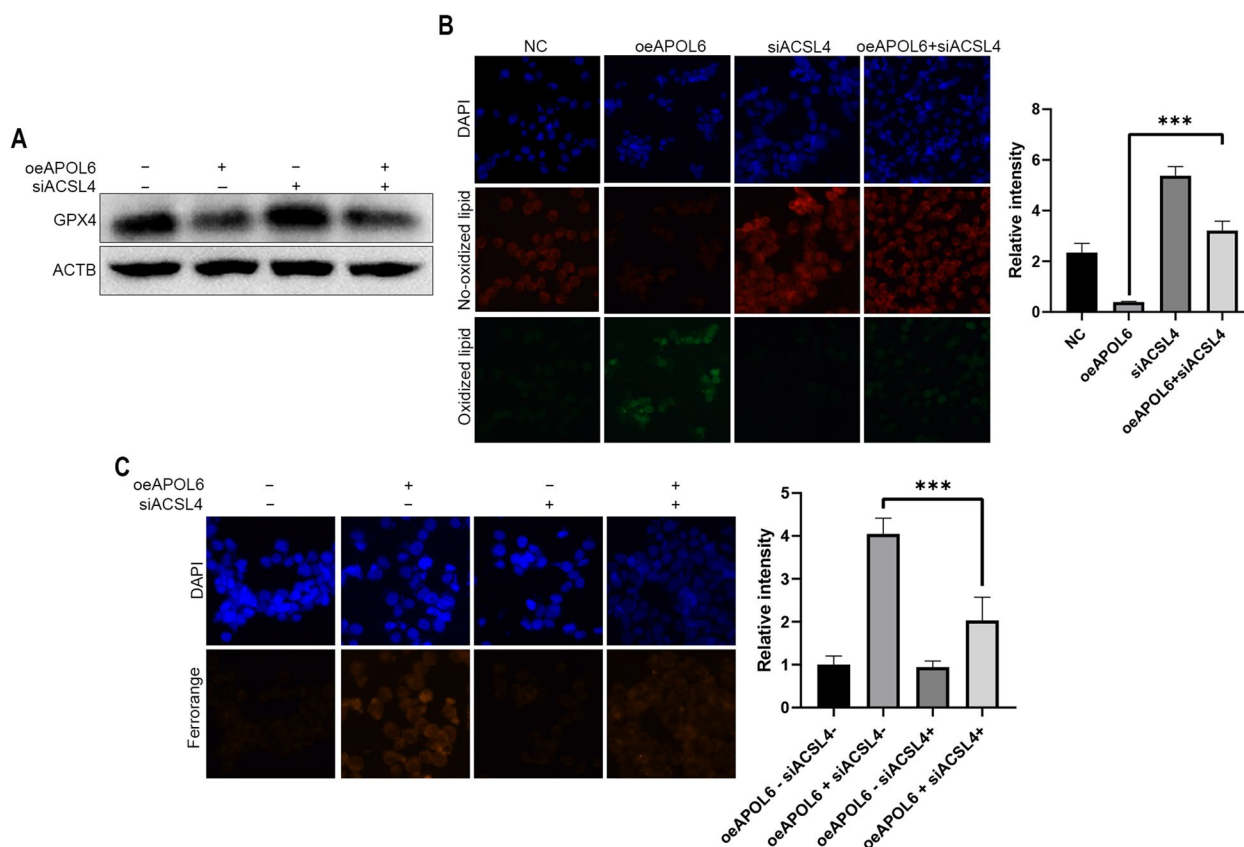


Fig. 8 APOL6 interacts with ACSL4 to promote ferroptosis in BLCA. **A** Western blot for GPX4 level. ACTB was employed as the loading control. **B** Levels of lipid peroxidation were expressed by C11-BODIPY581/591 probe. **C** Free iron levels were examined by FerroOrange probe

microenvironment and can act as a biomarker for immunologically ‘hot’ tumors.

In the current study, apart from BLCA, we found that APOL6 expression increased in patients responding to cancer immunotherapy in both BRCA and SKCM, and was associated with the immunomodulators of the TME in a publicly available cohort. In multiple cancers, the level of PD-L1 is used to predict the efficacy of immune checkpoint therapy [15]. However, in our studies of immunotherapy cohorts with BLCA, BRCA, and SKCM, we found that APOL6 has a similar, if not superior, ability to distinguish immunotherapy responses compared to PD-L1.

Ferroptosis, a form of iron-reliant programmed cell death, is defined by lipid peroxidation due to cellular metabolism and imbalanced redox homeostasis [46–48]. The accumulation of reactive oxygen species (ROS) enhances lipid peroxidation, thereby damaging cell membranes and ultimately leading to cell death. According to various studies, ferroptosis not only forms the basis of the onset and development of tumors but also plays a crucial role in antitumor therapy, including radiotherapy, chemotherapy, and immunotherapy [49, 50].

It has been reported that APOL6 level is positively connected with rectal cancer populations sensitive to radiotherapy [51]. We found that APOL6 is upregulated in the responder groups of BLCA, BRCA, and SKCM undergoing immune checkpoint therapy. Furthermore, the results in this report indicate that the overexpression of APOL6 promotes ferroptosis by decreasing the expression of GPX4 in BLCA. This suggests that ferroptosis may be a potential mechanism through which high APOL6 levels enhance tumor response to immunotherapy.

Furthermore, through artificial intelligence simulation and experimental verification, we observed an interaction between APOL6 and ACSL4 in BLCA cancer. Obviously, APOL6 acts as the promising biomarker and effective indicative effect for immunotherapy in BLCA by interacting with ACSL4.

Synthetic molecules can mimic the ferroptosis-inducing effects of IFN-γ on the Xc- system, offering a potential therapeutic strategy for targeting human and mouse tumor cell lines. Following IFN-γ stimulation, an increase in the phosphorylation of STAT1 and the expression levels of downstream genes IRF1 and APOL6 is observed in expanded potential stem cells (EPSC) derived from

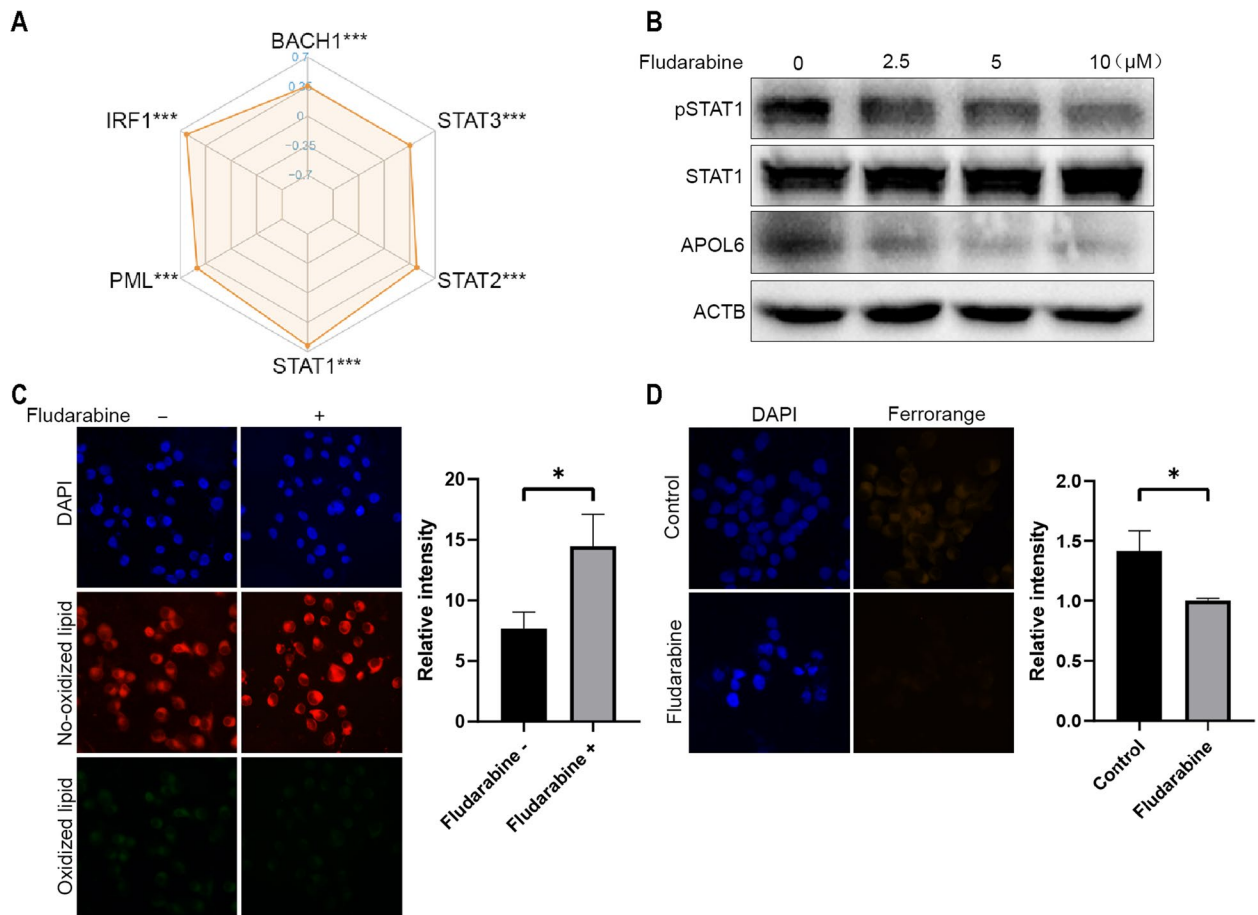


Fig. 9 The upstream key regulators of APOL6 involved in ferroptosis. **A** The radar chart showing the association between APOL6 and transcription factors. **B** After treated with fludarabine at 0, 2.5, 5, 10 μM, protein levels of STAT1, pSTAT1 and APOL6 in T24 cells were analyzed by western blot. **C** Following treatment with fludarabine, lipid peroxidation levels in T24 cells were measured by C11-BODIPY581/591 probe. **D** Free iron levels were examined after treating T24 cells as shown in (C) by FerroOrange probe

patients with certain innate immune deficiencies [52]. In this study, based on the Cistrome database, we predicted the direct upstream regulatory transcription factors of APOL6, among which STAT1 showed the highest correlation with APOL6, validated through NetworkAnalyst. Next, we also found that in BLCA, inhibition of phosphorylation of STAT1, suppressed the expression of APOL6. Despite the lack of a STAT1 binding site in the ACSL4 promoter region, studies have indicated that IFN- γ can still upregulate ACSL4 transcriptional expression in tumor cells. This regulation occurs through the activation of the JAK-STAT1 pathway, with IRF1 acting as a downstream mediator [53]. We speculate that IFN- γ , by promoting the phosphorylation of STAT1, may induce the upregulation of the downstream target gene APOL6, enhancing the interaction between APOL6 and ACSL4, and thereby promoting ferroptosis in BLCA. This could represent a novel potential mechanism by which APOL6 affects immunogenic cell death in tumor cells.

Despite its findings, this study leaves room for further investigation. Some limitations include the impact of APOL6 on the TME and immunotherapy requires further exploration. The prognostic significance of APOL6 in immunotherapy has only been validated in a limited cohort, which needs further verification in larger, more diverse cancer cohorts. The relationship between APOL6 and ferroptosis in BLCA, along with its potential molecular mechanisms, has not been totally explored through animal experiments. In summary, our research systematically analyzed the immunological correlation of APOL6 and its value in immunotherapy response. We found that APOL6 can act as a potential biomarker for BLCA and even other cancer patients who may benefit from immunotherapy, and discovered the STAT1/APOL6/GPX4 axis was the underlying regulating mechanism.

Supplementary Information

The online version contains supplementary material available at <https://doi.org/10.1186/s12885-024-12820-7>.

Supplementary Material 1: Figure S1. Hierarchical clustering of BLCA patients revealed two distinct immune subtypes. (A) Hierarchical clustering categorized BLCA patients into Immunity_H and Immunity_L using the ssGSEA method. (B) Overview of immune features and tumor immune microenvironment within the TCGA-BLCA cohort. (C) Validation of immunosubtype via tSNE. (D) Comparison of the ESTIMATEScore, ImmuneScore, and StromalScore between two subtypes. (E) Evaluation of differences in immune cell infiltration levels across two immunosubtypes. (F) The heatmap showing the DEGs between the Immunity_L and Immunity_H subtypes. (G) The heatmap showing the DEGs between samples from CR/PR and SD/PD groups in the IMvigor210 cohort. (H). The heatmap showing the DEGs between samples from the Alive group and Die group in the IMvigor210 cohort. (I) The intersection of DEGs in TCGA-BLCA cohort and IMvigor210 cohort. (J) KEGG enrichment analysis of the intersection DEGs in two BLCA datasets. Count representing the number of candidates.

Supplementary Material 2: Figure S2. Prognostic values of candidates in TCGA-BLCA cohort.

Supplementary Material 3: Figure S3. The impact of APOL6 on the immunological status in BLCA. (A) Enriched gene sets in KEGG collection by samples of high APOL6 expression. (B and C) Correlation between APOL6 expression and TIICs abundance.

Supplementary Material 4: Figure S4. APOL6 predicts an inflamed TME in BLCA. (A) Correlation between APOL6 and immunomodulators (chemokine, Immunoinhibitor, Immunostimulator, MHC, receptor) expression. (B) The heatmap showing the correlation between APOL6 and the activities of the various stages of the cancer-immunity cycle. (C) The relationship between APOL6 and TIICs abundance calculated relying on two algorithms (Timer, quanTlseq). (D) Different gene markers of prevalent TIICs between the low- and high-APOL6 groups.

Supplementary Material 5: Figure S5. Association between APOL6 and the immune phenotype in BLCA. (A) Different IPS levels in low- and high-APOL6 groups in BLCA. (B) Heatmap showing the link between APOL6 and immune-related targets in BLCA. (C) Heatmap showing the link between APOL6 and immune-related pathways. (D) Correlation between APOL6 expression and common inhibitory immune checkpoints.

Supplementary Material 6: Figure S6. Immuno-correlations between APOL6 and pan-cancer. (A) Pan-cancer analysis of correlations between APOL6 and 150 immunomodulators, including MHC, receptors, chemokines, immunoinhibitors, and immunostimulators. The color indicates the correlation coefficient. The asterisks denote notable differences. The asterisks indicate significant differences calculated by Pearson correlation test. (B) Associations between APOL6 and tumor purity in pan-cancer. (C) Correlation between APOL6 expression and TIICs abundance estimated by TIMER and quanTlseq algorithms in pan-cancer.

Supplementary Material 7: Figure S7. (A) Correlation between APOL6 expression and TIICs abundance analyzed by four algorithms. (B) Expression of APOL6 from samples between responders and non-responders in GSE104580. (C) Prediction of transcription factors for APOL6.

Supplementary Material 8.

Authors' contributions

Lei Liu and Xinyuan Zhao, as the corresponding authors, designed supervised the study. Zhiwei Fan, Yiting Liu and Xuehai Wang drafted the manuscript. Yuting Xu, Ruiyao Huang and Weijian Shi conducted the experiments. Yi Qu, Jialing Ruan and Chu Zhou were responsible for the analysis and visualization of the data. All authors have read and approved the published version of the manuscript.

Funding

This work was supported by National Natural Science Foundation of China (82200819), Natural Science Foundation of Jiangsu Province (BK20220605) and Jiangsu Innovative and Entrepreneurial Talent Programme (JSSCBS20211600).

Availability of data and materials

The data in this work will be available through the corresponding authors upon reasonable request.

Declarations

Ethics approval and consent to participate

Not applicable.

Consent for publication

Not applicable.

Competing interests

The authors declare no competing interests.

Received: 20 March 2024 Accepted: 16 August 2024

Published online: 26 August 2024

References

- Siegel RL, Giaquinto AN, Jemal A. Cancer statistics, 2024. *CA Cancer J Clin.* 2024;74(1):12–49.
- Cathomas R, Lorch A, Bruins HM, Comperat EM, Cowan NC, Efstathiou JA, et al. The 2021 updated European association of urology guidelines on metastatic urothelial carcinoma. *Eur Urol.* 2022;81(1):95–103.
- Liu H, Gu J, Jin Y, Yuan Q, Ma G, Du M, et al. Genetic variants in N6-methyladenosine are associated with bladder cancer risk in the Chinese population. *Arch Toxicol.* 2021;95(1):299–309.
- Gao J, Wang WQ, Pei Q, Lord MS, Yu HJ. Engineering nanomedicines through boosting immunogenic cell death for improved cancer immunotherapy. *Acta Pharmacol Sin.* 2020;41(7):986–94.
- Ni JJ, Zhang ZZ, Ge MJ, Chen JY, Zhuo W. Immune-based combination therapy to convert immunologically cold tumors into hot tumors: an update and new insights. *Acta Pharmacol Sin.* 2023;44(2):288–307.
- Pardoll DM. The blockade of immune checkpoints in cancer immunotherapy. *Nat Rev Cancer.* 2012;12(4):252–64.
- Wang Z, Zhang B, Zhang C, Ren S, Wang W, Wang Y, et al. Effect of region on the outcome of patients receiving PD-1/PD-L1 inhibitors for advanced cancer. *Int Immunopharmacol.* 2019;74:105709.
- Iwai Y, Ishida M, Tanaka Y, Okazaki T, Honjo T, Minato N. Involvement of PD-L1 on tumor cells in the escape from host immune system and tumor immunotherapy by PD-L1 blockade. *Proc Natl Acad Sci USA.* 2002;99(19):12293–7.
- Lenis AT, Lec PM, Chamie K, Mshs MD. Bladder cancer: a review. *JAMA.* 2020;324(19):1980–91.
- Yu EY, Petrylak DP, O'Donnell PH, Lee JL, van der Heijden MS, Loriot Y, et al. Enfortumab vedotin after PD-1 or PD-L1 inhibitors in cisplatin-ineligible patients with advanced urothelial carcinoma (EV-201): a multicentre, single-arm, phase 2 trial. *Lancet Oncol.* 2021;22(6):872–82.
- Gibney GT, Weiner LM, Atkins MB. Predictive biomarkers for checkpoint inhibitor-based immunotherapy. *Lancet Oncol.* 2016;17(12):e542–51.
- Topalian SL, Hodi FS, Brahmer JR, Gettinger SN, Smith DC, McDermott DF, et al. Safety, activity, and immune correlates of anti-PD-1 antibody in cancer. *N Engl J Med.* 2012;366(26):2443–54.
- Bejarano L, Jordao MJC, Joyce JA. Therapeutic Targeting of the Tumor Microenvironment. *Cancer Discov.* 2021;11(4):933–59.
- Zhou H, Zhang H, Shi M, Wang J, Huang Z, Shi J. A robust signature associated with patient prognosis and tumor immune microenvironment based on immune-related genes in lung squamous cell carcinoma. *Int Immunopharmacol.* 2020;88:106856.
- Galon J, Bruni D. Approaches to treat immune hot, altered and cold tumours with combination immunotherapies. *Nat Rev Drug Discov.* 2019;18(3):197–218.
- Rose TL, Weir WH, Mayhew GM, Shibata Y, Eulitt P, Uronis JM, et al. Fibroblast growth factor receptor 3 alterations and response to immune checkpoint inhibition in metastatic urothelial cancer: a real world experience. *Br J Cancer.* 2021;125(9):1251–60.

17. Puzstai L, Yau C, Wolf DM, Han HS, Du L, Wallace AM, et al. Durvalumab with olaparib and paclitaxel for high-risk HER2-negative stage II/III breast cancer: results from the adaptively randomized I-SPY2 trial. *Cancer Cell*. 2021;39(7):989–998. e985.
18. Wolf DM, Yau C, Wulfkuhle J, Brown-Swigart L, Gallagher RI, Lee PRE, et al. Redefining breast cancer subtypes to guide treatment prioritization and maximize response: predictive biomarkers across 10 cancer therapies. *Cancer Cell*. 2022;40(6):609–623. e606.
19. Gide TN, Quek C, Menzies AM, Tasker AT, Shang P, Holst J, et al. Distinct immune cell populations define response to Anti-PD-1 monotherapy and anti-PD-1/Anti-CTLA-4 combined therapy. *Cancer Cell*. 2019;35(2):238–255. e236.
20. Necchi A, Joseph RW, Loriot Y, Hoffman-Censits J, Perez-Gracia JL, Petrylak DP, et al. Atezolizumab in platinum-treated locally advanced or metastatic urothelial carcinoma: post-progression outcomes from the phase II IMvigor210 study. *Ann Oncol*. 2017;28(12):3044–50.
21. Zheng R, Wan C, Mei S, Qin Q, Wu Q, Sun H, et al. Cistrome Data Browser: expanded datasets and new tools for gene regulatory analysis. *Nucleic Acids Res*. 2019;47(D1):D729–35.
22. Hänzelmann S, Castelo R, Guinney J. GSVA: gene set variation analysis for microarray and RNA-seq data. *BMC Bioinformatics*. 2013;14:7.
23. Bindea G, Mlecnik B, Tosolini M, Kirilovsky A, Waldner M, Obenauf AC, et al. Spatiotemporal dynamics of intratumoral immune cells reveal the immune landscape in human cancer. *Immunity*. 2013;39(4):782–95.
24. Maaten LVD, Hinton GE. Visualizing data using t-SNE. *J Mach Learn Res*. 2008;9:2579–605.
25. Yoshihara K, Shahmoradgoli M, Martinez E, Vegesna R, Kim H, Torres-Garcia W, et al. Inferring tumour purity and stromal and immune cell admixture from expression data. *Nat Commun*. 2013;4:2612.
26. Newman AM, Liu CL, Green MR, Gentles AJ, Feng W, Xu Y, et al. Robust enumeration of cell subsets from tissue expression profiles. *Nat Methods*. 2015;12(5):453–7.
27. Racle J, de Jonge K, Baumgaertner P, Speiser DE, Gfeller D. Simultaneous enumeration of cancer and immune cell types from bulk tumor gene expression data. *eLife*. 2017;6:e26476.
28. Becht E, Giraldo NA, Lacroix L, Buttard B, Elarouci N, Petitprez F, et al. Estimating the population abundance of tissue-infiltrating immune and stromal cell populations using gene expression. *Genome Biol*. 2016;17(1):249.
29. Finotello F, Mayer C, Platner C, Laschober G, Rieder D, Hackl H, et al. Molecular and pharmacological modulators of the tumor immune contexture revealed by deconvolution of RNA-seq data. *Genome Med*. 2019;11(1):34.
30. Liu XS, Li B, Chen Q, Li J, Cohen D, Zeng Z, et al. TIMER2.0 for analysis of tumor-infiltrating immune cells. *Nucleic Acids Res*. 2020;48(W1):W509–14.
31. Liberzon A, Birger C, Thorvaldsdóttir H, Ghandi M, Mesirov Jill P, Tamayo P. The molecular signatures database hallmark gene set collection. *Cell Syst*. 2015;1(6):417–25.
32. Chen DS, Mellman I. Oncology meets immunology: the cancer-immunity cycle. *Immunity*. 2013;39(1):1–10.
33. Charoentong P, Finotello F, Angelova M, Mayer C, Efremova M, Rieder D, et al. Pan-cancer immunogenomic analyses reveal genotype-immunophenotype relationships and predictors of response to checkpoint blockade. *Cell Rep*. 2017;18(1):248–62.
34. Weng G, Wang E, Wang Z, Liu H, Zhu F, Li D, et al. HawkDock: a web server to predict and analyze the protein-protein complex based on computational docking and MM/GBSA. *Nucleic Acids Res*. 2019;47(W1):W322–30.
35. Desta IT, Porter KA, Xia B, Kozakov D, Vajda S. Performance and its limits in rigid body protein-protein docking. *Structure (London, England: 1993)*. 2020;28(9):1071–1081. e1073.
36. Jumper J, Evans R, Pritzel A, Green T, Figurnov M, Ronneberger O, et al. Highly accurate protein structure prediction with AlphaFold. *Nature*. 2021;596(7873):583–9.
37. Ylilauri M, Pentikainen OT. MMGBSA as a tool to understand the binding affinities of filamin-peptide interactions. *J Chem Inf Model*. 2013;53(10):2626–33.
38. Zhou G, Soufan O, Ewald J, Hancock REW, Basu N, Xia J. NetworkAnalyst 3.0: a visual analytics platform for comprehensive gene expression profiling and meta-analysis. *Nucleic Acids Res*. 2019;47(W1):W234–41.
39. Zhao X, Wu Y, Li J, Li D, Jin Y, Zhu P, et al. JNK activation-mediated nuclear SIRT1 protein suppression contributes to silica nanoparticle-induced pulmonary damage via p53 acetylation and cytoplasmic localisation. *Toxicology*. 2019;423:42–53.
40. Bretz AC, Parnitzke U, Kronthaler K, Dreker T, Bartz R, Hermann F, et al. Domatinostat favors the immunotherapy response by modulating the tumor immune microenvironment (TIME). *J Immunother Cancer*. 2019;7(1):294.
41. Sweis RF, Spranger S, Bao R, Paner GP, Stadler WM, Steinberg G, et al. Molecular drivers of the non-T-cell-inflamed tumor microenvironment in urothelial bladder cancer. *Cancer Immunol Res*. 2016;4(7):563–8.
42. Liu Z, Lu H, Jiang Z, Pastuszyn A, Hu CA. Apolipoprotein I6, a novel proapoptotic Bcl-2 homology 3-only protein, induces mitochondria-mediated apoptosis in cancer cells. *Mol Cancer Res*. 2005;3(1):21–31.
43. Smith EE, Malik HS. The apolipoprotein L family of programmed cell death and immunity genes rapidly evolved in primates at discrete sites of host-pathogen interactions. *Genome Res*. 2009;19(5):850–8.
44. Alspach E, Lussier DM, Schreiber RD. Interferon gamma and Its Important roles in promoting and inhibiting spontaneous and therapeutic cancer immunity. *Cold Spring Harb Perspect Biol*. 2019;11(3):a028480.
45. Zhaorigetu S, Yang Z, Toma I, McCaffrey TA, Hu CA. Apolipoprotein L6, induced in atherosclerotic lesions, promotes apoptosis and blocks Beclin 1-dependent autophagy in atherosclerotic cells. *J Biol Chem*. 2011;286(31):27389–98.
46. Dixon SJ, Lemberg KM, Lamprecht MR, Skouta R, Zaitsev EM, Gleason CE, et al. Ferroptosis: an iron-dependent form of nonapoptotic cell death. *Cell*. 2012;149(5):1060–72.
47. Wang Y, Zhang Z, Sun W, Zhang J, Xu Q, Zhou X, et al. Ferroptosis in colorectal cancer: potential mechanisms and effective therapeutic targets. *Biomed Pharmacother*. 2022;153:113524.
48. Fan Z, Cai L, Wang S, Wang J, Chen B. Baicalin prevents myocardial ischemia/reperfusion injury through inhibiting ACSL4 mediated ferroptosis. *Front Pharmacol*. 2021;12:628988.
49. Zhao L, Zhou X, Xie F, Zhang L, Yan H, Huang J, et al. Ferroptosis in cancer and cancer immunotherapy. *Cancer Commun (Lond)*. 2022;42(2):88–116.
50. Sun Y, Berleth N, Wu W, Schlutermann D, Deitersen J, Stuhldreier F, et al. Fin56-induced ferroptosis is supported by autophagy-mediated GPX4 degradation and functions synergistically with mTOR inhibition to kill bladder cancer cells. *Cell Death Dis*. 2021;12(11):1028.
51. Liu Y, Yang Y, Ni F, Tai G, Yu C, Jiang X, et al. Research on radiotherapy related genes and prognostic target identification of rectal cancer based on multi-omics. *J Transl Med*. 2023;21(1):856.
52. Liu X, Chan VS, Smith KG, Ming C, Or CS, Tsui FT, et al. Recapitulating primary immunodeficiencies with expanded potential stem cells: proof of concept with STAT1 gain of function. *J Allergy Clin Immunol*. 2024;153(4):1125–39.
53. Liao P, Wang W, Wang W, Kryczek I, Li X, Bian Y, et al. CD8(+) T cells and fatty acids orchestrate tumor ferroptosis and immunity via ACSL4. *Cancer Cell*. 2022;40(4):365–378. e366.

Publisher's Note

Springer Nature remains neutral with regard to jurisdictional claims in published maps and institutional affiliations.